The impact of defect scattering on the quasi-ballistic transport of nanoscale conductors

I. S. Esqueda, C. D. Cress, Y. Cao, Y. Che, M. Fritze, and C. Zhou

Citation: Journal of Applied Physics **117**, 084319 (2015); doi: 10.1063/1.4913779
View online: http://dx.doi.org/10.1063/1.4913779
View Table of Contents: http://scitation.aip.org/content/aip/journal/jap/117/8?ver=pdfcov
Published by the AIP Publishing

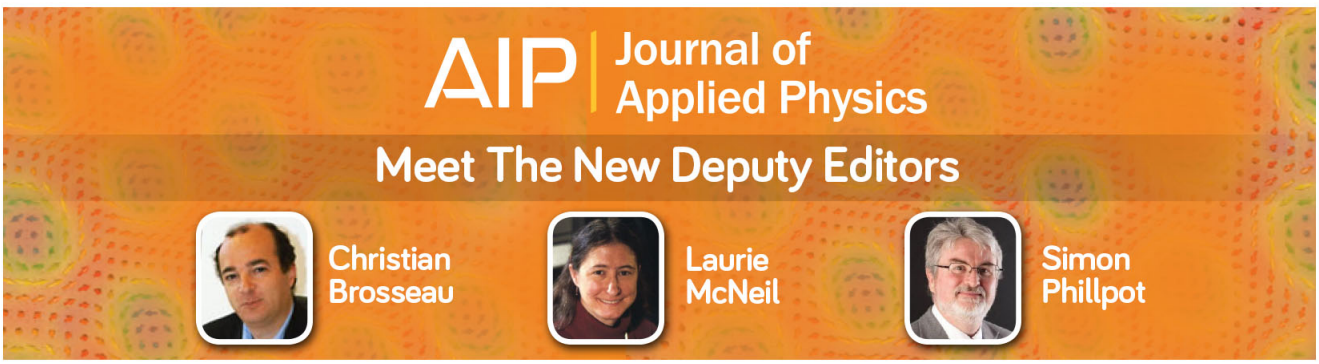

JOURNAL OF APPLIED PHYSICS **117**, 084319 (2015)

The impact of defect scattering on the quasi-ballistic transport of nanoscale conductors

I. S. Esqueda,[1,a)] C. D. Cress,[2] Y. Cao,[3] Y. Che,[3] M. Fritze,[1] and C. Zhou[3]
[1]*Information Sciences Institute, University of Southern California, Marina del Rey, California 90292, USA*
[2]*Electronics Science and Technology Division, Naval Research Laboratory, Washington, DC 20375, USA*
[3]*Department of Electrical Engineering, University of Southern California, Los Angeles, California 90089, USA*

(Received 12 December 2014; accepted 18 February 2015; published online 27 February 2015)

Using the Landauer approach for carrier transport, we analyze the impact of defects induced by ion irradiation on the transport properties of nanoscale conductors that operate in the quasi-ballistic regime. Degradation of conductance results from a reduction of carrier mean free path due to the introduction of defects in the conducting channel. We incorporate scattering mechanisms from radiation-induced defects into calculations of the transmission coefficient and present a technique for extracting modeling parameters from near-equilibrium transport measurements. These parameters are used to describe degradation in the transport properties of nanoscale devices using a formalism that is valid under quasi-ballistic operation. The analysis includes the effects of bandstructure and dimensionality on the impact of defect scattering and discusses transport properties of nanoscale devices from the diffusive to the ballistic limit. We compare calculations with recently published measurements of irradiated nanoscale devices such as single-walled carbon nanotubes, graphene, and deep-submicron Si metal-oxide-semiconductor field-effect transistors. © *2015 AIP Publishing LLC*. [http://dx.doi.org/10.1063/1.4913779]

INTRODUCTION

The scaling of metal-oxide-semiconductor field-effect transistors (MOSFETs) and the introduction of novel materials have allowed the fabrication of nanoscale transistors that operate near the ballistic limit.[1] In nanoscale devices, carrier scattering results from interactions with charged impurities, lattice defects, phonons, and with other charged carriers.[2] Scattering theory describes the steady state current in a nanoscale conductors using a transmission coefficient that captures the probability that some of the injected carriers will backscatter in the channel and not contribute to charge conduction.[3–6] However, as the channel length (L) is reduced to a dimension comparable to the backscattering mean free path (λ), carriers will transit the channel undergoing fewer scattering events. Mathematically this is described with the transmission coefficient approaching unity in the ballistic limit (i.e., when $L \ll \lambda$). However, most modern devices operate in a regime $L \sim \lambda$ and the transport is said to be quasi-ballistic.

Recent techniques based on the Landauer theory have been demonstrated for modeling quasi-ballistic transport in nanoscale devices.[7–10] These techniques express current in the presence of scattering using a transmission coefficient that is related to λ that can be extracted from measurements of long-channel devices as described in Ref. 8. Analyzing the effects of radiation-induced defects on the quasi-ballistic transport properties of nanoscale devices, based on these techniques, requires incorporating the relevant defect scattering mechanisms into calculations of current (or conductance).

In this paper, we analyze and model the impact of radiation-induced defects on the transport properties of nanoscale devices using the Landauer-Büttiker theory. This approach is valid from the diffusive to the ballistic limit and applied here to studying the impact of defect scattering on quasi-ballistic transport. Experimental studies have demonstrated the impact of radiation-induced lattice defects on the electrical characteristics of various nanoscale devices and materials through irradiation with energetic particles including electrons, protons, and heavy ions. These studies include thin silicon layers in SOI devices and deep-submicron bulk MOSFETs,[11–15] carbon-based materials and nanoscale devices such as graphene[16–18] and carbon nanotubes (CNTs),[19–23] and III–V compound semiconductors heterojunctions and high electron-mobility transistors (HEMTs).[24–26] Fig. 1(a) illustrates radiation-induced defects scattering of electron in a 2D graphene sheet.

The analysis and modeling approach presented in this paper extends conventional techniques for describing radiation-induced transport degradation based on drift-diffusion theory that use effective carrier mobility[27–30] to the ballistic limit by using scattering theory and transmission coefficients. We also discuss how bandstructure and dimensionality relate to the impact of defect scattering on conductance. Other contributions of this work include the development and demonstration of analytical modeling techniques for the quasi-ballistic conductivity as a function the defect scattering, channel length, and carrier density in silicon, graphene, and CNTs. All of the analysis presented in this work are validated with recently published experimental data and relate not only to applications intended for radiation environments but also to transport characterization and nanofabrication techniques that utilize particle irradiation. We note that the presented analysis and modeling approach is

a)E-mail: isanchez@isi.edu

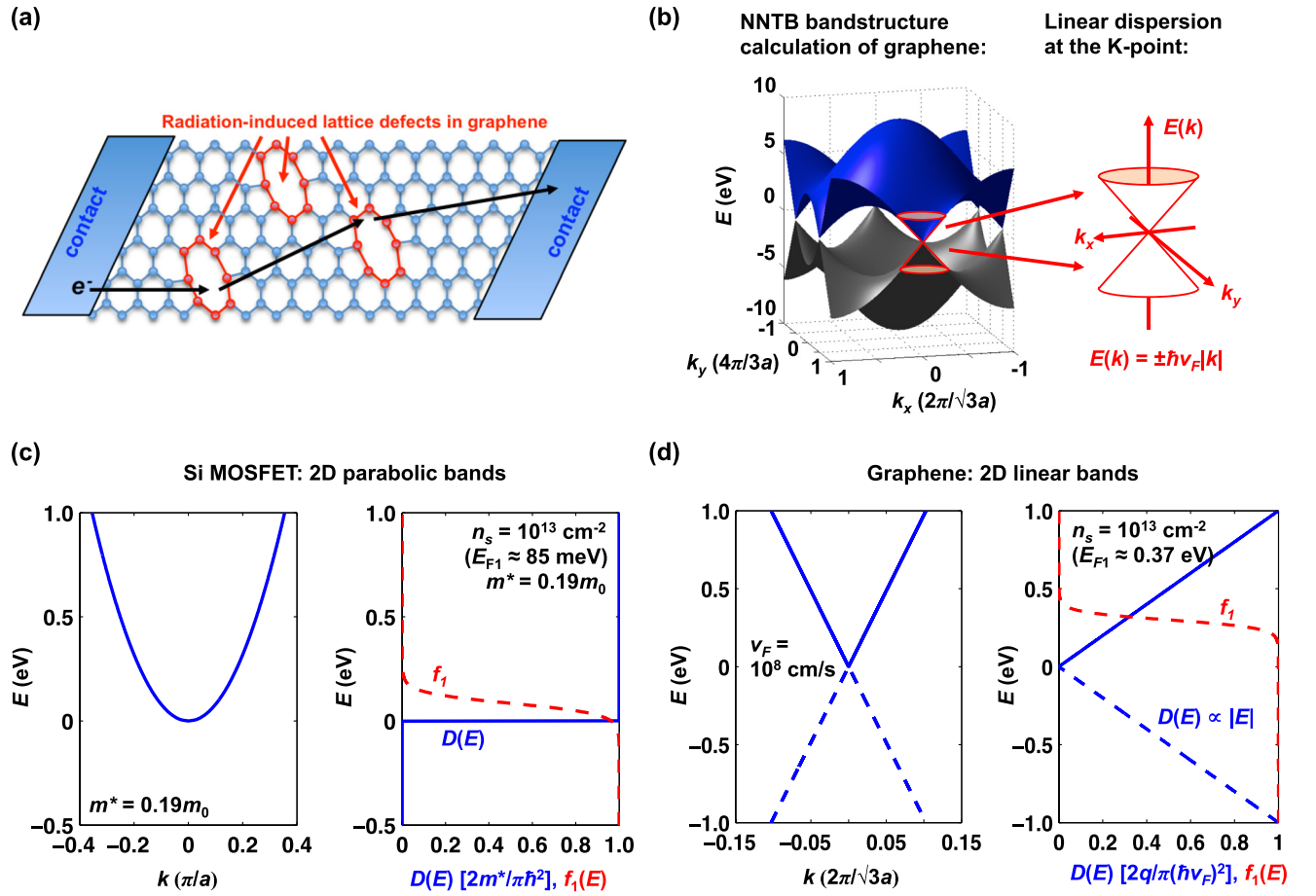

FIG. 1. (a) Illustration of radiation-induced defect scattering of electrons in graphene. (b) NNTB bandstructure calculation of graphene and simplified linear dispersion at the K-points for energies near the intrinsic Fermi level. (c) Bandstructure, $D(E)$ and Fermi-function $f_1 = f(E_{F1})$ used for a 2D channel with parabolic bands in the inversion layer of a Si MOSFET. Energy is referenced to E_{C0}, $n_s = 10^{13}\,\mathrm{cm}^{-2}$ and $V_{ds} = 50\,\mathrm{mV}$. (d) Calculations of the linear bandstructure, $D(E)$ and f_1 in graphene for $n_s = 10^{13}\,\mathrm{cm}^{-2}$ and $V_{ds} = 50\,\mathrm{mV}$.

generally applicable to studying the impact of scattering on the transport properties of nanoscale conductors, whereas irradiation allows the controlled introduction of structural defects.

MODELING APPROACH

Applying the Landauer-Büttiker theory to a nanoscale device allows expressing the steady state current as

$$I = \frac{2q}{h}\int T(E)M(E)\left[f_1(E) - f_2(E)\right]dE, \tag{1}$$

where q is the electronic charge, h is Planck's constant, $T(E)$ is the transmission coefficient, $M(E)$ is the number of transporting channels (or modes), and $f_1(E)$ and $f_2(E)$ are the Fermi functions in the source and drain contacts, respectively.[3,5] Scattering theory can be used to relate the transmission coefficient to the mean free path for backscattering (λ) resulting in

$$T(E) = \frac{\lambda(E)}{\lambda(E) + L}, \tag{2}$$

where L is the channel length.[5] This expression for $T(E)$ is valid from the diffusive limit (i.e., when $L \gg \lambda$, $T \approx \lambda/L \ll 1$) to the ballistic limit (i.e., when $L \ll \lambda$, $T \to 1$) and for the quasi-ballistic transport regime (i.e., $L \approx \lambda$, $T < 1$). The number of conducting channels $M(E)$ is proportional to the density of states $D(E)$ and to the average velocity in the positive direction of transport $\langle v_x^+(E)\rangle$. Additionally, it is proportional to the width (W) for 2D channels and to the cross-sectional area (A) for 3D channels. For the case of a 2D channel,

$$M(E) = W\frac{h}{4}\langle v_x^+(E)\rangle D(E). \tag{3}$$

The Fermi functions at the source and drain contacts are, respectively, given by $f_1 = f(E, E_{F1})$ and $f_2 = f(E, E_{F2})$, where E_{F1} and E_{F2} are the Fermi energy levels at the source and drain contacts, and

$$f(E, E_F) = \frac{1}{e^{(E-E_F)/k_BT_L} + 1}. \tag{4}$$

In (4), k_B is the Boltzmann constant and T_L is the temperature of the lattice. Using (1)–(4) allows demonstrating the impact of radiation-induced defects on the transport properties of quasi-ballistic nanoscale devices. Increased scattering from radiation-induced defects reduces $\lambda(E)$, lowering the current and channel conductance $G = I/V$ of the device due to a reduction of the transmission probability. The impact of a

reduced mean free path for backscattering on transmission probability has a dependence on L as given by (2). In this work, we use numerical calculations of (1)–(4) to analyze the impact of radiation-induced defect scattering on the quasi-ballistic transport characteristics of nanoscale Si MOSFETs, graphene, and single-walled CNTs (SWCNTs).

The analysis presented in this work utilizes calculations of coherent transport that capture well the properties at the dimensions of interests (i.e., nanoscale devices) and for the scattering mechanisms being considered (i.e., elastic, phase-conserving processes). However, quantum interference effects are not incorporated in calculations for (wide) 2D channels as the large number of conducting modes results in a localization length $L_0 \sim M\lambda \gg L$ placing them within the weakly localized regime.[5] For the case of single-mode conduction in 1D channels, the localization length $L_0 \sim \lambda$ can be considerably reduced by the introduction of radiation-induced defects resulting in strong localization when $L \sim L_0$. In this regime, quantum interference becomes significant resulting in an exponential dependence of channel conductance on L.[5] These quantum effects have been shown experimentally on SWCNTs[19] and are further discussed in Sec. III.

RESULTS AND DISCUSSION

In the Si MOSFET, the charge-conducting carriers are confined to a thin inversion layer that can be modeled as a 2D channel with parabolic bands using an effective mass approximation. For electrons in the conduction band, we can express the kinetic energy as

$$E(k) - E_{C0} = \frac{\hbar^2\left(k_x^2 + k_y^2\right)}{2m^*}. \tag{5}$$

In (5), we are considering electrons in the lowest sub-band that is two fold degenerate as a result of quantum confinement and has a conduction band minimum at energy E_{C0} with an effective mass $m^* = m_t = 0.19m_0$. The density of states in 2D is given by

$$D(E) = (2)\frac{m^*}{\pi\hbar^2}H(E - E_{C0}), \tag{6}$$

where the factor of 2 accounts for sub-band degeneracy and H is the Heaviside step function. For this band structure, the average $+x$ velocity is given by

$$\langle v_x^+(E)\rangle = \frac{2}{\pi}v(E) = \frac{2}{\pi}\sqrt{\frac{2(E - E_{C0})}{m^*}}. \tag{7}$$

Using (3), (6), and (7), we obtain $M(E)$ for a 2D channel with parabolic bands as

$$M(E) = \frac{2W}{\pi\hbar}\sqrt{2m^*(E - E_{C0})}. \tag{8}$$

The mean free path for backscattering can be modeled in a power law form for some common scattering mechanisms[2] and is expressed as

$$\lambda(E) = \lambda_0\left(\frac{E - E_{C0}}{k_B T_L}\right)^s. \tag{9}$$

In (9), λ_0 is a constant independent of energy and the exponential term s depends on dimensionality, bandstructure, and the scattering mechanism. Radiation-induced lattice defects are modeled as short-range potential scattering centers with a scattering rate (i.e., $1/\tau(E)$) that is proportional to the density of states. For a 2D channel with parabolic bands, this corresponds to $\lambda(E) \propto v(E)\tau(E) \propto (E - E_{C0})^{1/2}$, therefore $s = 1/2$. Increased scattering from radiation-induced defects is modeled as a reduction in λ_0.

Calculations of I and G in a 2D Si MOSFET inversion layer can be done numerically using (1). These calculations require the position of the Fermi levels at the source and drain contacts for determining f_1 and f_2. For a fixed sheet carrier density n_s, E_{F1} and $E_{F2} = E_{F1} - qV_{ds}$ are obtained by solving

$$n_s = N_c F_0(E_{F1})/2 + N_c F_0(E_{F1} - qV_{ds})/2, \tag{10}$$

where $N_c = 2m^* k_B T_L/\pi\hbar^2$, V_{ds} is the drain-to-source voltage, and $F_0(E_F)$ is the Fermi-Dirac integral of order zero. Fig. 1(c) summarizes the energy-dependent parameters used in the numerical calculations of 2D conductors. Fig. 1(c) plots the lowest doubly degenerate parabolic band in a 2D Si MOSFET channel, and also plots $D(E)$ and $f_1(E, E_{F1})$, referenced to E_{C0}, with an inverted axis allowing direct comparison with the bandstructure plot. We note that the electrostatic impact from ionizing radiation charge trapping effects in gate oxides (e.g., threshold voltage shifts) is captured in n_s and the corresponding shifts in the Fermi levels.

Fig. 2 plots channel conductance as a function of L for a sheet carrier density of $n_s = 10^{13}\,\mathrm{cm}^{-2}$ and for $V_{ds} = 50\,\mathrm{mV}$. This value of n_s is typical for a Si MOSFET in strong inversion and is consistent with extractions from the data shown in Fig. 2. The calculations of G are given for decreasing λ_0 (i.e., reduction of defect scattering mean free path) and are normalized to the ballistic conductance (G_{ball}) that corresponds to $T(E) = 1$. Also shown in Fig. 2 are the extractions

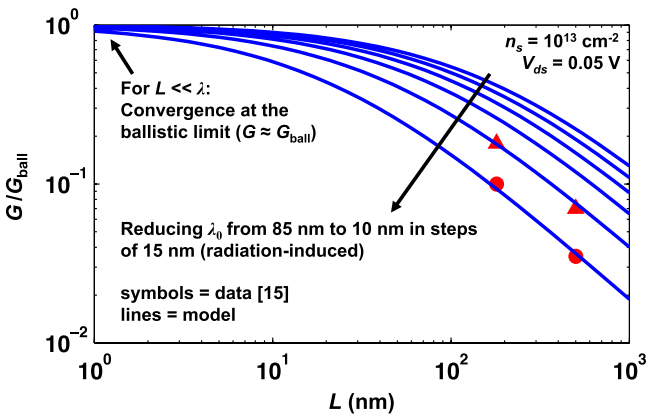

FIG. 2. Calculations of normalized conductance vs. channel length in the 2D inversion layer of a Si MOSFET with increasing (radiation-induced) defect scattering mechanisms compared to experimental extractions from Ref. 15. Extractions are from low-field, strong inversion I-V measurements of n-channel MOSFETs before (triangles) and after (circles) heavy ion irradiation.

of G/G_{ball} from experimental data on ion irradiated deep submicron Si MOSFETs from Ref. 15. The results in Fig. 2 demonstrate the impact of defect scattering on the quasi-ballistic transport properties of a 2D channel with parabolic bands as described the Landauer theory. Reducing L relative to the energy-averaged $\lambda(E)$ increases G towards the ballistic limit as transmission increases due to a reduction in the backscattering probability. For devices with long (i.e., diffusive) channels, G is directly proportional to $\lambda(E)$ allowing us to extract its radiation-dependence that can be used for modeling the response under quasi-ballistic transport in scaled devices. We also notice that the calculations and extractions of G scale as $1/L$ under diffusive transport (i.e., when $L \gg \lambda$) consistent with a weakly localized regime ($L \ll L_0 = M\lambda$).

The bandstructure of graphene can be obtained using a nearest-neighbor tight-binding (NNTB) formalism that provides a simple, closed-form expression with demonstrated accuracy in reproducing first-principle calculations at low energies. The NNTB energy dispersion of graphene is given by

$$E(k) = \pm\gamma\sqrt{1 + 4\cos\left(\frac{\sqrt{3}a}{2}k_x\right)\cos\left(\frac{a}{2}k_y\right) + 4\cos^2\left(\frac{a}{2}k_y\right)}, \tag{11}$$

where k_x and k_y are the Brillouin zone wavevector x and y components, $a = \sqrt{3}a_{C-C}$ where $a_{C-C} = 1.42\,\text{Å}$ is the carbon-carbon bond length, and γ is the nearest-neighbor overlap energy ($\sim$3 eV).[31] The bandstructure has a linear dispersion near the intrinsic Fermi energy, where the conduction and valence bands intersect at the K-points (i.e., the Dirac points; see Fig. 1(b)). For this low-energy range, we have

$$E(k) = \pm\hbar v_F k = \pm\hbar v_F\sqrt{k_x^2 + k_y^2}, \tag{12}$$

where the electron velocity $v(k) = \hbar^{-1}\partial E/\partial k = v_F \approx 10^8\,\text{cm/s}$ is a constant independent of energy.[32] Using (12), we obtain $\langle v_x^+(E)\rangle = 2v_F/\pi$ and $D(E) = 2|E|/\pi(\hbar v_F)^2$, allowing expressing the density of modes in graphene as

$$M(E) = \frac{2W|E|}{\pi\hbar v_F}. \tag{13}$$

By substituting (13) into (1), we obtain the conductance in a graphene sheet as

$$G = \frac{I}{V} = \frac{2qW}{v_F(\hbar\pi)^2 V_{ds}}\int\left(\frac{\lambda(E)}{\lambda(E)+L}\right)|E|\left[f_1(E) - f_2(E)\right]dE. \tag{14}$$

Fig. 1(d) plots the bandstructure and density of states used for calculations of radiation-induced degradation of conductance in graphene. Short-range scattering from radiation-induced defects in graphene can be modeled using (9) with a corresponding exponential term of $s = -1$.[33] This proportionality results from $\lambda(E) \propto 1/D(E) \propto 1/E$.

Fig. 3 plots calculations of the sheet conductance (or conductivity) $\sigma = G(L/W)$ as a function of E_{F1} using (14).

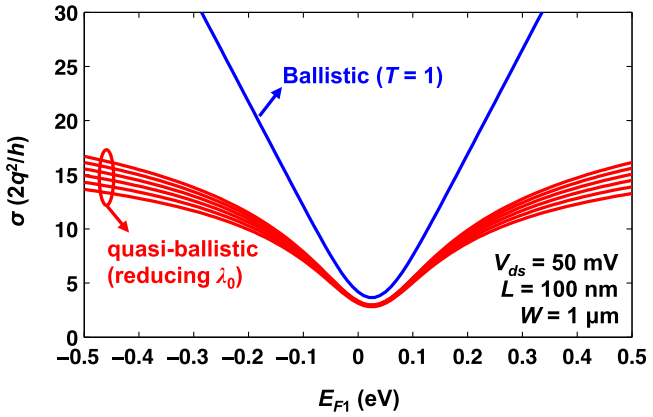

FIG. 3. Calculations of sheet conductance in graphene as a function of E_{F1} for the ballistic and quasi-ballistic cases using (14) where $\sigma = G(L/W)$. The quasi-ballistic case shows the impact of increased short-range elastic scattering from radiation-induced lattice defects where $\lambda(E)$ is given by (9) and $s = -1$. In the quasi-ballistic calculations, λ_0 varies from 1000 to 750 nm in steps of 50 nm.

These results demonstrate the impact of increased short-range scattering from radiation-induced lattice defects on the quasi-ballistic transport properties of graphene. The ballistic sheet conductance is also shown in Fig. 3 for comparison. As shown in Fig. 3, the ballistic conductance increases linearly with energy since it is directly proportional to $M(E)$. Introducing scattering from radiation-induced defects reduces the sheet conductance as observed in the quasi-ballistic calculations. At $|E_{F1}| < 0.1$ eV, the conductance remains linear and reduced λ_0 has little effect, while at $|E_{F1}| > 0.1$ eV, the conductance is no longer linear and the impact of reducing λ_0 becomes more apparent because $\lambda(E) \propto 1/E$. To better understand the quasi-ballistic response in graphene, we consider the diffusive and ballistic limits where $T \approx \lambda/L$ and $T = 1$ respectively, and solve for the near-equilibrium (i.e., low-field) sheet conductance. For low-field transport (i.e., low V_{ds}) the difference $(f_1 - f_2) \approx (\partial f/\partial E_F)(qV_{ds})$ and the sheet conductance can be expressed as

$$\sigma_{ball} = L\left(\frac{2q^2}{h}\right)\left(\frac{2k_BT_L}{\pi\hbar v_F}\right)[\ln(1 + e^{\eta_F})], \tag{15}$$

$$\sigma_{diff} = \lambda_0\left(\frac{2q^2}{h}\right)\left(\frac{2k_BT_L}{\pi\hbar v_F}\right)\left(\frac{1}{1 + e^{-\eta_F}}\right), \tag{16}$$

where $\eta_F = E_F/k_BT_L$. The derivation for (15) and (16) is given in the Appendix. From (15) and (16), it can be seen that σ_{ball} varies linearly with energy and that σ_{diff} is constant for $E \gtrsim 3k_BT_L$ (i.e., σ_{diff} is independent of E and n_s). In general, the energy dependence of $\lambda(E)$ for the scattering mechanism being considered will determine the energy dependence of σ_{diff}. The expressions for sheet conductance in (15) and (16) are interpreted as the product of the quantum of conductance, the number of channel in the Fermi window, and the average mean free path. For quasi-ballistic transport, the sheet conductance is estimated using Mathiessen's Rule as

$$\frac{1}{\sigma} \approx \frac{1}{\sigma_{ball}} + \frac{1}{\sigma_{diff}}. \tag{17}$$

The total sheet conductance is limited by σ_{ball} and σ_{diff}, respectively, at the ballistic and diffusive limits and is given by (17) for the intermediate range. For example, in the calculations shown in Fig. 3, σ_{diff} varied from ~25 to ~18 $[2q^2/h]$ limiting the total sheet conductance at the higher $|E|$ ranges.

Experimental investigations on ion-irradiated graphene sheets have shown that short-rage scattering mechanisms that result in a carrier density independent conductivity are mostly unaffected by dose[16] and are significant only at high energies.[17] Instead, a conductivity component that is linearly dependent on carrier density is significantly degraded with radiation.[16,18] This is attributed to the creation of midgap states as a result from radiation-induced disorder in the graphene lattice.[18] In the Landauer-Büttiker approach, such scattering mechanisms correspond to a mean free path for backscattering given by (9) with $s=1$. In this case, λ increases with energy as higher energy carriers scatter less from the potential fluctuations created by lattice defects. Following the same procedure used to obtain (15) and (16), the (defect-limited) sheet conductance is given by

$$\sigma_{def} = \left(\frac{2q^2}{h}\right)\left(\frac{2k_BT_L}{\pi\hbar v_F}\right)\lambda_0 F_1(\eta_F), \tag{18}$$

where $F_1(E_F)$ is the Fermi-Dirac integral of order one. For graphene, the sheet carrier density is given by

$$n_s(E_F) = \int D(E)f(E,E_F)dE = \frac{2}{\pi}\left(\frac{k_BT_L}{\hbar v_F}\right)^2 F_1(\eta_F). \tag{19}$$

It is clear form comparing (18) and (19) that σ_{def} varies linearly with n_s. In Figs. 4 and 5, we compare experimental data from ion-irradiated graphene samples,[16] with calculations of conductivity. Fig. 4 plots fits of σ_{def} given by (18) as a function of n_s given by (19) against data from long-channel (i.e., diffusive) exfoliated graphene samples irradiated at low temperature (41 K) in ultra high vacuum (UHV) using 500 eV Ne and He ions. The carrier density for the experimental data is estimated using $n_s \approx (C_{ox}/q)(V_g - V_{min})$, where

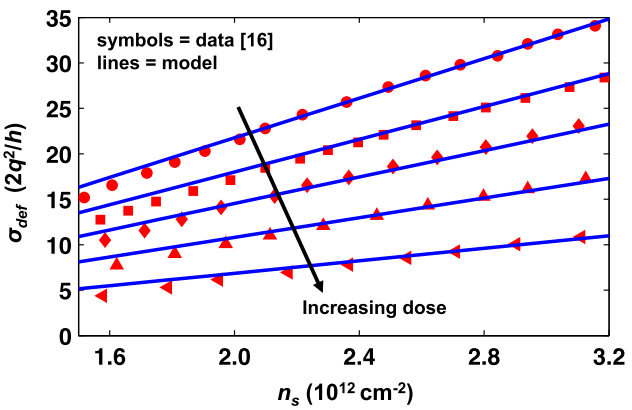

FIG. 4. Fits of σ_{def} given by (18) as a function of n_s given by (19) against data from long-channel (i.e., diffusive) exfoliated graphene samples irradiated at low temperature (41 K) in UHV using 500 eV Ne and He ions. In these calculations λ_0 varies from 6 to 2 nm in steps of ~1 nm. We note that the energy-averaged mean free path $\langle\lambda(E)\rangle$ varies form ~160 nm to ~50 nm at $n_s = 3\times10^{12}\,\mathrm{cm}^{-2}$. This is consistent with estimates of distance between defects made in Ref. 16 using Raman spectra.

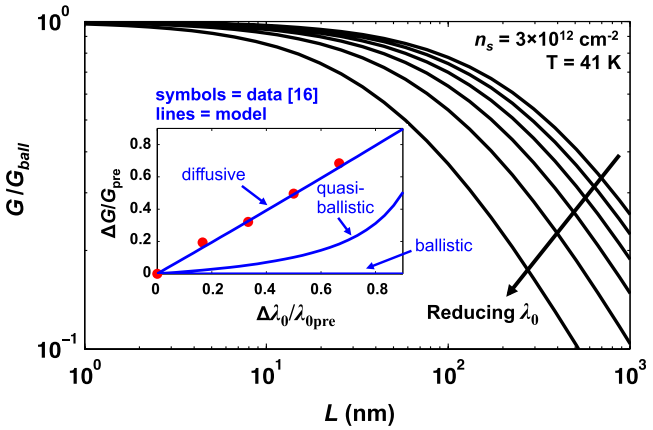

FIG. 5. Normalized conductance (G/G_{ball}) vs. L for $n_s = 3\times10^{12}\,\mathrm{cm}^{-2}$ using λ_0 from the fits to experimental data shown in Fig. 4. Inset plots calculations of relative change in G as a function of the relative change in λ_0 for the diffusive ($\lambda \ll L$), ballistic ($\lambda \gg L$), and quasi-ballistic ($\lambda \sim L$) case. G_{pre} and λ_{0pre} are the values G and λ_0 before irradiation.

V_{min} is the gate voltage at the minimum conductivity. The impact of radiation-induced defect scattering on the low-field conductance of graphene can now be numerically evaluated up to the ballistic limit using (14) and $\lambda(E)$ obtained from the fits to the experimental data. Fig. 5 plots the normalized conductance (G/G_{ball}) as a function of channel length for a fixed $n_s = 3\times10^{12}\,\mathrm{cm}^{-2}$ and using the values of λ_0 used to fit the experimental results. The inset in Fig. 5 plots calculations of relative change in G as a function of the relative change in λ_0 for the diffusive ($\lambda \ll L$), ballistic ($\lambda \gg L$), and quasi-ballistic ($\lambda \sim L$) case. As expected, the experimental data matches well with the calculations in the case of diffusive transport. We note that the values of backscattering mean free path used to fit the data are consistent with estimates of distance between defects made in Ref. 16 from Raman spectra. At $n_s = 3\times10^{12}\,\mathrm{cm}^{-2}$, the energy-averaged mean free path $\langle\lambda(E)\rangle$ varies form ~160 nm before irradiation to ~50 nm after irradiation.

So far we have considered the impact of radiation-induced defects on the quasi-ballistic transport properties of 2D inversion layers in the channels of Si MOSFETs with parabolic bands and in 2D graphene sheets with linear energy dispersion. Calculations of G/G_{ball} that incorporate defect scattering demonstrate similar effects in both cases. However, even for irradiated graphene samples, the mobility $\mu = (1/q)(d\sigma/dn_s)$ approximately varied between 5000 and 1800 cm^2/V-s which is greater than effective channel mobilities measured in Si MOSFETs by approximately an order of magnitude. The high carrier mobilities measured on irradiated graphene samples alludes to the general interests for high-performance nanoelectronics. Considering radiation-induced defects in graphene, measurements reveal degradation of a sheet conductance component that is directly proportional to n_s. Given the bandstructure of graphene this corresponds to $\lambda(E) \propto E$ and $G \propto E^2$. Therefore, high-energy carriers in graphene experience less scattering from radiation-induced lattice defects and have a smaller impact on G/G_{ball}. We will now consider the impact of dimensionality by analyzing radiation-induced defect scattering in 1D channels of SWCNTs.

In SWCNTs, quantization of the allowed wavevectors resulting from boundary conditions on the Bloch functions restricts transport to 1D sub-bands. The 1D sub-bands are quantized along the circumferential direction of the nanotube, but continuous along the axial direction. In metallic tubes the lowest energy sub-band crosses a K-point and can be described with a linear dispersion (similar to graphene) expressed as $E = \pm\hbar v_F|k|$. The linear E-k relationship results in an constant (i.e., energy-independent) density of states $D(E) = D_0$ and single-mode conduction for 1D metallic SWCNTs.

For radiation-induced defect scattering in 1D metallic SWCNTs, we have $\lambda(E) \propto \tau(E) \propto 1/D(E) \propto \lambda_0$ (i.e., energy independent scattering rates[34]). Therefore, solving (1) for the low-field conductance in 1D metallic SWCNT gives

$$G = \frac{I}{V} = \frac{4q^2}{h}\left(\frac{\lambda_0}{\lambda_0 + L}\right)\left(\frac{1}{1 + e^{-\eta_F}}\right), \tag{20}$$

where the factor of 4 comes from spin and valley degeneracy and $G \rightarrow (4q^2/h)[\lambda_0/(\lambda_0 + L)]$ for $\eta_F \gg 1$ (i.e., for degenerate conductors). For $L \ll \lambda_0$, we have $G \approx G_{ball} = 4q^2/h$ and is independent of L, and for $L \gg \lambda_0$ we have $G \approx G_{ball}(\lambda_0/L)$ and scales as $1/L$ (i.e., ohmic-behavior). However, recent experiments have showed that for single-mode phase-coherent conduction in 1D metallic SWCNTs the low-field resistance increased exponentially with L revealing strong localization and quantum interference effects.[19] Additionally, these experiments showed that ion-irradiation reduced the localization length, since $L_0 \sim \lambda$, and therefore, increased the resistance of the 1D conductors.

Using standard Green's function techniques for quantum transport allows simulating the exponential dependence of G on L as a function of defect density.[19] In this work we attempt to analytically interpret and model the impact of radiation-induced defect scattering mechanisms on the quasi-ballistic properties of nanoscale devices. Therefore, we include a comparison of calculations for the low-field conductance using (20) and extractions from the data to demonstrate the deviation from the diffusive ohmic-like behavior expected for a weakly localized regime, and to interpret the shifts in the transition from a ballistic to a strongly localized regime as a function of L. Figure 6 plots extractions of G from the low-voltage resistance measurements of ion irradiated metallic SWCNT in Ref. 19 (symbols) compared to calculations of conductance using (20) (dashed lines) and to analytical fits to the experiments using an exponential dependence on L (solid lines). For the analytical fits $G = G_{ball}\exp(-L/L_0)$, where L_0 is the localization length that ranges from ~225 to ~70 nm and is consistent with the previous work. The comparison in Fig. 6 reveals the discrepancy between the ohmic-like behavior expected for a weakly localized regime and the experiments confirming the relevance of quantum interference effects in single-mode conduction of 1D channels.

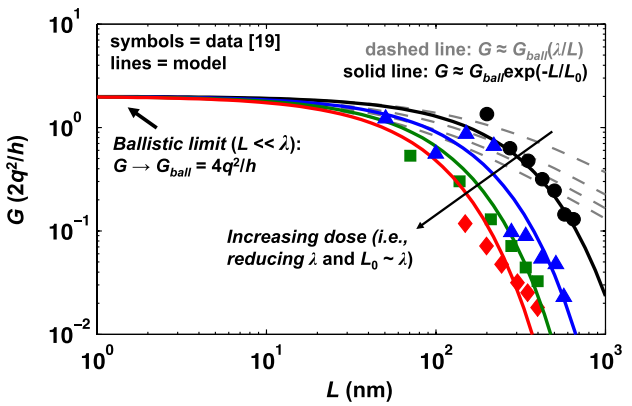

FIG. 6. Extractions of G from the low-voltage resistance measurements of ion irradiated metallic SWCNT in Ref. 19 (symbols) compared to calculations of conductance using (20) (dashed lines) and to analytical fits to the experiments using an exponential dependence on L (solid lines).

CONCLUSIONS

The impact of radiation-induced defects on the quasi-ballistic transport properties of nanoscale conductors is analyzed and model using numerical and analytical calculations of conductance based on the Landauer-Büttiker theory. The analysis presented in this paper is valid from the diffusive to the ballistic limit and uses scattering theory to model the impact of defects on conductance through calculations of backscattering mean free path and transmission coefficient. This approach incorporates bandstructure and dimensionality and is validated with experimental data from recently published work on silicon, graphene, and carbon nanotubes.

For 2D conductors we describe the quasi-ballistic transport as a function of L with a conductance transitioning from the ballistic limit to the diffusive regime with ohmic-like (i.e., $1/L$) dependence. This is consistent with phase coherent transport in devices with nanoscale channel lengths, but weak localization due to a large number of conducting channels (proportional to W and E). Radiation-induced point defects are modeled as short-range potentials that introduce scattering rates proportional to the density of states. For the linear dispersion in 2D graphene this results in a conductance that is independent of n_s. However, experiments in graphene reveal a negligible response in the n_s-independent sheet conductance as a function of dose. Instead, a sheet conductance component that varies linearly with n_s is strongly affected by radiation. This is attributed to radiation-induced disorder in the lattice of graphene and corresponds to $\lambda(E) \propto E$ and $G \propto E^2$. Thus, highly degenerate graphene carriers are expected to experience less scattering from radiation-induced defects and have a reduced impact on G/G_{ball}. This is consistent with the large ion fluence (or defect density) required to significantly lower conductivity by more than 1 order of magnitude experimentally in graphene.[16,18]

In SWCNT with 1D channels and single mode conductance, quantum interference results in an exponential dependence of G on L as was recently shown experimentally. This is consistent with phase coherent transport and a strongly localized regime. Additionally, the localization length $L_0 \sim \lambda$ is reduced by the introduction of radiation-induced lattice defects. Using recently published data from Ref. 19, we compare calculations of conductance with experimental extractions to demonstrate the deviation from the diffusive ohmic-like behavior expected for a weakly localized regime

and to interpret the shifts in the transition from a ballistic to a strongly localized regime as a function of channel length.

ACKNOWLEDGMENTS

This work was supported (in part) by the Defense Threat Reduction Agency, Basic Research Award Nos. HDTRA-1-10-1-0015 and HDTRA-1-10-1-0122.

APPENDIX: DERIVATION OF GRAPHENE ANALYTICAL CONDUCTIVITIES

For low-field transport in graphene using the approximation $(f_1 - f_2) \approx (\partial f/\partial E_F)(qV_{ds})$, we can express the conductance as

$$G = \frac{I}{V} = \frac{2q^2}{h}\int T(E)\left(\frac{2WE}{\pi\hbar v_F}\right)\left(\frac{\partial f}{\partial E_F}\right)dE. \quad \text{(A1)}$$

In the case of ballistic transport $T(E) = 1$ and ballistic sheet conductance $\sigma_{ball} = G_{ball}(L/W)$ is given by

$$\begin{aligned}\sigma_{ball} &= \frac{L}{W}\frac{2q^2}{h}\int\left(\frac{2WE}{\pi\hbar v_F}\right)\left(\frac{\partial f}{\partial E_F}\right)dE \\ &= L\frac{2q^2}{h}\frac{2}{\pi\hbar v_F}\frac{\partial}{\partial E_F}\left[\int\frac{EdE}{1+e^{(E-E_F)/k_BT_L}}\right]. \quad \text{(A2)}\end{aligned}$$

Changing variables by defining $\eta = E/k_BT_L$ and $\eta_F = E_F/k_BT_L$ gives

$$\begin{aligned}\sigma_{ball} &= L\frac{2q^2}{h}\frac{2k_BT_L}{\pi\hbar v_F}\frac{\partial}{\partial\eta_F}\left[\int\frac{\eta d\eta}{1+e^{\eta-\eta_F}}\right] \\ &= L\frac{2q^2}{h}\frac{2k_BT_L}{\pi\hbar v_F}\frac{\partial}{\partial\eta_F}\left[F_1(\eta_F)\right] \\ &= L\frac{2q^2}{h}\frac{2k_BT_L}{\pi\hbar v_F}F_0(\eta_F) \\ &= L\frac{2q^2}{h}\frac{2k_BT_L}{\pi\hbar v_F}\left[\ln(1+e^{\eta_F})\right]. \quad \text{(A3)}\end{aligned}$$

In (A3), we have made use of the Fermi-Dirac integral property that reduces its order by one when differentiated with respect to its argument. Using the analytical expression for $F_0(\eta_F)$ we obtain σ_{ball} as given by (15). For the diffusive case, we have $T(E) \approx \lambda(E)/L$ and the sheet conductance $\sigma_{diff} = G_{diff}(L/W)$ is given by

$$\begin{aligned}\sigma_{diff} &= \frac{L}{W}\frac{2q^2}{h}\int\frac{\lambda(E)}{L}\left(\frac{2WE}{\pi\hbar v_F}\right)\left(\frac{\partial f}{\partial E_F}\right)dE \\ &= \lambda_0\frac{2q^2}{h}\frac{2k_BT_L}{\pi\hbar v_F}\frac{\partial}{\partial E_F}\left[\int\frac{dE}{1+e^{(E-E_F)/k_BT_L}}\right], \quad \text{(A4)}\end{aligned}$$

where we have used $\lambda(E) = \lambda_0(E/k_BT_L)^{-1}$. Changing variables by defining $\eta = E/k_BT_L$ and $\eta_F = E_F/k_BT_L$ gives

$$\begin{aligned}\sigma_{diff} &= \lambda_0\frac{2q^2}{h}\frac{2k_BT_L}{\pi\hbar v_F}\frac{\partial}{\partial\eta_F}\left[\int\frac{d\eta}{1+e^{\eta-\eta_F}}\right] \\ &= \lambda_0\frac{2q^2}{h}\frac{2k_BT_L}{\pi\hbar v_F}\frac{\partial}{\partial\eta_F}\left[F_0(\eta_F)\right] \\ &= \lambda_0\frac{2q^2}{h}\frac{2k_BT_L}{\pi\hbar v_F}F_{-1}(\eta_F) \\ &= \lambda_0\frac{2q^2}{h}\frac{2k_BT_L}{\pi\hbar v_F}\left(\frac{1}{1+e^{-\eta_F}}\right). \quad \text{(A5)}\end{aligned}$$

In (A5), we have used the analytical expression for $F_{-1}(\eta_F)$ to obtain σ_{diff} as expressed in (16).

[1]M. Lundstrom, "Elementary scattering theory of the Si MOSFET," IEEE Electron Device Lett. **18**(7), 361–363 (1997).
[2]M. Lundstrom, *Fundamentals of Carrier Transport* (Cambridge University Press, Cambridge, UK, 2009).
[3]R. Landauer, "Conductance as a consequence of incident flux," IBM J. Res. Dev. **1**, 223 (1957).
[4]J. P. McKelvey, R. L. Longini, and T. P. Brody, "Alternative approach to the solution of added carrier transport problems in semiconductors," Phys. Rev. **123**, 51–57 (1961).
[5]S. Datta, *Electronic Transport in Mesoscopic Structures* (Cambridge University Press, Cambridge, UK, 1995).
[6]M. Lundstrom and Z. Ren, "Essential physics of carrier transport in nanoscale MOSFETs," IEEE Trans. Electron Devices **49**(1), 133–141 (2002).
[7]M. Lundstrom and J.-H. Rhew, "A Landauer approach to nanoscale MOSFETs," J. Comput. Electron. **1**(4), 481–489 (2002).
[8]C. Jeong, D. A. Antoniadis, and M. S. Lundstrom, "On backscattering and mobility in nanoscale silicon MOSFETs," IEEE Trans. Elec. Devices **56**(11), 2762–2768 (2009).
[9]M. Lundstrom and D. A. Antoniadis, "Compact models and the physics of nanoscale FETs," IEEE Trans. Electron Devices **61**(2), 225–233 (2014).
[10]R. Kim, S. Datta, and M. Lundstrom, "Influence of dimensionality on thermoelectric device performance," J. Appl. Phys. **105**(3), 034506 (2009).
[11]F. Tan, X. An, L. Huang, X. Zhang, and R. Huang, "Heavy-ion-induced permanent damage in ultra-deep submicron fully depleted SOI devices," in *IEEE 11th International Conference on Solid-State and Integrated Circuit Technology (ICSICT)* (2012), p. 1.
[12]K. D. Shcherbachev, V. T. Bublik, V. N. Mordkovich, and D. M. Pazhin, "Specific features of formation of radiation defects in the silicon layer in SOI structures," Fiz. Tekh. Poluprovodn. **45**(6), 754–758 (2011).
[13]A. Griffoni, S. Gerardin, A. Cester, A. Paccagnella, E. Simoen, and C. Claeys, "Effects of heavy-ion strikes on fully depleted SOI MOSFETs with ultra-thin gate oxide and different strain-inducing techniques," IEEE Trans. Nucl. Sci. **54**(6), 2257–2263 (2007).
[14]S. Xue, R. Huang, P. Wang, W. Wang, D. Wu, Y. Pei, and X. Zhang, "Impact of proton-radiation-induced spacer damage on the dc characteristics degradation in deep-submicron metal-oxide-semiconductor field effect transistors," J. Appl. Phys. **105**, 084505 (2009).
[15]X. Shou-Bin, H. Ru, H. De-Tao, W. Si-Hao, T. Fei, W. Jian, A. Xia, and Z. Xing, "Impact of the displacement damage in channel and source/drain regions on the DC characteristics degradation in deep-submicron MOSFETs after heavy ion irradiation," Chin. Phys. B **19**(11), 117307 (2010).
[16]J.-H. Chen, W. G. Cullen, C. Jang, M. S. Fuhrer, and E. D. Williams, "Defect scattering in graphene," Phys. Rev. Lett. **102**(23), 236805 (2009).
[17]C. Jang, S. Adam, J.-H. Chen, E. D. Williams, S. Das Sarma, and M. S. Fuhrer, "Tuning the effective fine structure constant in graphene: Opposing effects of dielectric screening on short- and long-range potential scattering," Phys. Rev. Lett. **101**(14), 146805 (2008).
[18]G. Buchowicz, P. R. Stone, J. T. Robinson, C. D. Cress, J. W. Beeman, and O. D. Dubon, "Correlation between structure and electrical transport in ion-irradiated graphene grown on Cu foils," App. Phys. Lett. **98**, 032102 (2011).
[19]C. Gomez-Navarro, P. J. De Pablo, J. Gomez-Herrero, B. Biel, F. J. Garcia-Vidal, A. Rubio, and F. Flores, "Tuning the conductance of single-walled carbon nanotubes by ion irradiation in the Anderson localization regime," Nat. Mater. **4**, 534–539 (2005).
[20]A. T. Lee, Y.-J. Kang, and K. J. Chang, "Transport properties of carbon nanotubes: Effects of Vacancy Clusters and Disorder," J. Phys. Chem. C **116**, 1179–1184 (2012).
[21]A. V. Krasheninnikov, K. Nordlund, M. Sirvio, E. Salonen, and J. Keinonen, "Formation of ion-irradiation-induced atomic-scale defects on walls of carbon nanotubes," Phys. Rev. B **63**, 245405 (2001).
[22]W.-K. Hong, C. Lee, D. Nepal, and K. E. Geckeler, "Radiation hardness of the electrical properties of carbon nanotube network field effect transistors under high-energy proton irradiation," Nanotechnology **17**(2), 5675–5680 (2006).
[23]J. E. Rossi, C. D. Cress, A. R. Helenic, C. M. Schauerman, R. A. DiLeo, N. D. Cox, S. R. Messenger, B. D. Weaver, S. M. Hubbard, and B. J. Landi, "Ion irradiation of electronic-type-separated single wall carbon

nanotubes: A model for radiation effects in nanostructured carbon," J. Appl. Phys. **112**, 034314 (2012).
[24]H.-Y. Kim, C. F. Lo, L. Liu, F. Ren, J. Kim, and S. J. Pearton, "Proton-irradiated InAlN/GaN high electron mobility transistors at 5, 10, and 15 MeV energies," Appl. Phys. Lett. **100**, 012107 (2012).
[25]B. D. Weaver and E. M. Jackson, "Universal behavior in irradiated high-electron mobility transistors," Appl. Phys. Lett. **80**(15), 2791–2793 (2002).
[26]C. F. Lo, C. Y. Chang, B. H. Chu, H.-Y. Kim, J. Kim, D. A. Cullen, L. Zhou, D. J. Smith, S. J. Pearton, A. Dabiran, B. Cui, P. P. Chow, S. Jang, and F. Ren, "Proton irradiation effects on AlN/GaN high electron mobility transistors," J. Vac. Sci. Technol. B **28**(5), L47 (2010).
[27]D. Zupac, K. F. Galloway, R. D. Schrimpf, and P. Augier, "Radiation-induced mobility degradation in p-channel double-diffused metal-oxide-semiconductor power transistors at 300 and 77 K," J. Appl. Phys. **73**(15), 2910–2915 (1993).
[28]N. Stojadinović, S. Golubović, V. Davidović, and S. Djoric-Veljkovic, "Modeling of radiation-induced mobility degradation in MOSFETs," in *Proceedings of the 21st International Conference on Microelectronics* (1997), pp. 355–356.
[29]A. P. Gnana Prakash, S. C. Ke, and K. Siddappa, "High-energy radiation effects on subthreshold characteristics, transconductance and mobility of n-channel MOSFETs," Semicond. Sci. Technol. **18**(12), 1037–1042 (2003).
[30]A. Cester, S. Gerardin, A. Paccagnella, J. R. Schwank, G. Vizkelethy, A. Candelori, and G. Ghidini, "Drain current decrease in MOSFETs after heavy ion irradiation," IEEE Trans. Nucl. Sci. **51**(6), 3150–3157 (2004).
[31]R. Saito, G. Dresselhaus, and M. S. Dresselhaus, *Physical Properties of Carbon Nanotubes* (Imperial, London, 1998).
[32]K. Geim and K. S. Novoselov, "The rise of graphene," Nat. Mater. **6**, 183–191 (2007).
[33]S. Das Sarma and E. H. Hwang, "Universal density scaling of disorder-limited low-temperature conductivity in high-mobility two-dimensional systems," Phys. Rev. B **88**, 035439 (2013).
[34]A. Javey, J. Guo, M. Paulsson, Q. Wang, D. Mann, M. Lundstrom, and H. Dai, "High-field quasiballistic transport in short carbon nanotubes," Phys. Rev. Lett. **92**(10), 106804 (2004).